Highlighting research results from Mechanics, Materials and Computing group and Soft Machines Lab at Carnegie Mellon University, Pittsburgh, USA and Soft and Nanoscale Materials group at Northeastern University, Boston, USA.

Gelation and mechanical response of patchy rods

We perform Brownian dynamics simulations to study the gelation of suspensions of attractive, rod-like particles. We show that if the attraction is sufficiently corrugated or patchy, over time, a rigid space-spanning network will form. Surprisingly, the structural and mechanical properties are non-monotonic in the fraction of the surface that is allowed to bind.

ROYAL SOCIETY OF CHEMISTRY

www.softmatter.org

Registered charity number: 207890

Soft Matter

PAPER

Gelation and mechanical response of patchy rods†

Navid Kazem,[a] Carmel Majidi[b] and Craig E. Maloney*[c]

We perform Brownian dynamics simulations to study the gelation of suspensions of attractive, rod-like particles. We show that in detail the rod–rod surface interactions can dramatically affect the dynamics of gelation and the structure and mechanics of the networks that form. If the attraction between the rods is perfectly smooth along their length, they will collapse into compact bundles. If the attraction is sufficiently corrugated or patchy, over time, a rigid space-spanning network will form. We study the structure and mechanical properties of the networks that form as a function of the fraction of the surface, *f*, that is allowed to bind. Surprisingly, the structural and mechanical properties are non-monotonic in *f*. At low *f*, there are not a sufficient number of cross-linking sites to form networks. At high *f*, rods bundle and form disconnected clusters. At intermediate *f*, robust networks form. The elastic modulus and yield stress are both non-monotonic in the surface coverage. The stiffest and strongest networks show an essentially homogeneous deformation under strain with rods re-orienting along the extensional axis. Weaker, more clumpy networks at high *f* re-orient relatively little with strong non-affine deformation. These results suggest design strategies for tailoring surface interactions between rods to yield rigid networks with optimal mechanical properties.

1 Introduction

Rods often aggregate in suspension. The rods may be made out of a broad array of materials: polymers, bio-polymers, viruses, or inorganics (ceramics or metals). The competing driving forces for dispersion and aggregation are also diverse: surface charges, depletion interactions, van der Waals forces, *etc.* These materials are important for a vast array of technologies (opto-electronics,[1–4] structural composites[5–14] *etc.*), and naturally occurring materials like xanthan gum[15] and wood pulp.[16] In some cases, the rod aggregates form disconnected clusters which enhance the viscosity of the suspension, but fail to gel into a solid. In other cases, the aggregates form rigid, space-spanning networks, and the suspension takes on solid-like properties. Despite the large number of materials that fall into this class, structure formation and resulting properties are still not well understood.

Rod network formation is a particularly interesting challenge. Physical gelation is still not well understood even for spheres.[17–20] Neither are the non-equilibrium and non-linear properties of even purely repulsive rods.[21–24] Network aggregation may be slow and

can display glass-like dynamics.[25–27] The process can be effectively athermal (binding energies are typically many times *kT*) and controlled by kinetics, much like diffusion limited aggregation (DLA), and understanding the equilibrium state will probably not lead to a better understanding of the strongly out-of-equilibrium aggregates.

In general, colloidal suspensions of uncharged particles are unstable to aggregation. Much work has gone into stabilizing uncharged rods by chemically functionalizing them with grafted polymers or by introducing surfactants at appropriate concentrations. Particular examples include: carbon nano-tubes (CNTs),[10–14,25,28–60] colloidal minerals like boehmite,[26,61–67] inorganic nano-rods like gold,[1–4,68–71] nanocrystalline cellulose,[8,9,72–77] and FD virus.[7,61,78–82] Despite this large body of experimental work, theory/simulation/modeling of structure formation, dynamics, and response has been lacking. Some previous theory/simulation results have focused on related areas: detailed physical chemistry of surface interactions between rods and adsorbing polymers;[44,48,52,54] non-linear rheology of hard, repulsive rods/fibers;[22–24] non-linear rheology of sticky rods;[83] equilibrium phase behavior of attractive rods;[84,85] mechanical properties of statically-cross-linked networks of rigid rods[26,46] and semi-flexible fibers;[86,87] diffusion limited aggregation (DLA) of hard, attractive rods.[88] However, surprisingly little numerical work has focused on aggregation itself.

Our goal here is to introduce a minimal model for network formation and mechanical response. We are interested in the

[a] Carnegie Mellon University, Civil and Environmental Engineering, Pittsburgh, PA, USA. E-mail: nkazem@andrew.cmu.edu
[b] Carnegie Mellon University, Mechanical Engineering, Pittsburgh, PA, USA. E-mail: cmajidi@andrew.cmu.edu
[c] Northeastern University, Mechanical and Industrial Engineering, Boston, MA, USA. E-mail: c.maloney@neu.edu

regime where the inter-rod surface interactions are strong so that the rods are effectively athermal and the rods are far above the critical volume fraction necessary for the percolation of a rigid network but still far below the isotropic to nematic transition. One key insight we have gained in constructing a minimal model is that in order for rigid networks to form, the rods must have some sort of irregularity in the surface interactions. If the attraction is uniform, in the regime of volume fractions we study, the rods always aggregate into disconnected clusters and can never form a spanning network or support a static load. On the other hand, if the interactions are corrugated or patchy, then the tendency for bundling is defeated and one can, over time, form rigid, space-spanning networks.

In this work, we introduce a simple model for the patchiness by distributing a number of attractive sites at random along each rod. These discrete attractive sites may be thought of as defects where stabilizing grafted or physically adsorbed polymers are missing or at a locally low concentration. Alternatively, in systems where attractive interactions are governed by the explicit addition of ligands on the surface, we may consider the sticking sites to be locations where there are ligands and the non-sticking sites to be patches where ligands are missing. The central result is that increasing the fraction, f, of the surface which is attractive has a non-intuitive, non-montonic effect on the structure and mechanics of the networks which form. For small f, there are too few attractive sites along the rods to form robust networks. As f increases, at first, the networks become increasingly rigid and strong with more and more cross links between rods at attractive sites and essentially a homogeneous structure. However, as more and more of the surface become attractive, branches of the networks become bundled, the structure becomes more heterogeneous, there are fewer and fewer load bearing paths, and the elastic modulus and yield stress go down. Finally at large enough f, the networks completely fall apart into disconnected bundles.

2 Models and protocols

In Fig. 1 we present our interaction model. We consider that a fraction of the surface has been functionalized to prevent attractive interactions, but the remaining fraction, f, remains attractive. Rods of length L are treated as beads, spaced along a line at a spacing a. Attractive sites along the rod are modeled using a standard Lennard-Jones (LJ) interaction with characteristic length, σ, and energy, ε_{LJ}. Purely repulsive sites are modeled with the Weeks–Chandler–Anderson (WCA) potential with the same σ and energy of $\varepsilon_{LJ}/100$.‡ Two rods can then bind only at sites that are attractive on both rods. The dimensionless parameters in the model are: $L/\sigma = 20$ (aspect ratio), $\varepsilon_{LJ}/kT = 10$ (binding energy), $a/\sigma = 0.4$ (corrugation parameter), $\phi \approx 0.02$ (rod volume fraction), f (fraction of surface which is attractive). For $L/\sigma = 20$ and $\phi \approx 0.02$, the system is well below the hard-rod nematic transition.[85,89] We use a standard Brownian dynamics algorithm which neglects

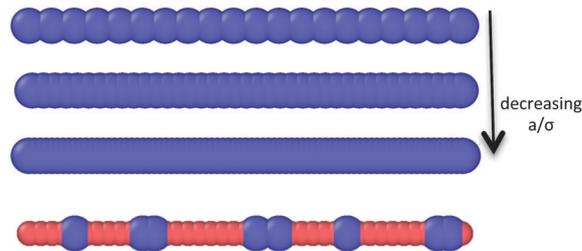‡ The purely repulsive WCA potential is simply the LJ potential cut off at the point of zero force.

Fig. 1 Schematic of the interaction model. Rods of length L are modeled as a collection of beads along a line with spacing a. Blue beads are attractive LJ particles with a characteristic length of σ and interaction strength ε_{LJ}. Red beads are repulsive WCA particles with $\sigma = \sigma_{LJ}$ and $\varepsilon = \varepsilon_{LJ}/100$. We denote the fraction of blue, binding beads as f.

hydrodynamic interactions between the rods. A more detailed hydrodynamical treatment could be implemented using dissipative particle dynamics or some other coarse-grained representation of the solvent particles if desired. All lengths reported below are in units of σ, and all times in units of τ, the diffusion time for a bead.

Since the bond strength is $\varepsilon_{LJ} = 10kT$, bonds will never break once formed, and our systems can be considered athermal. In this sense, the dynamics are similar to DLA.[88] However, there is a crucial distinction. In our model, once a cross-link forms, rods are free to pivot. If there are adjacent attractive sites, the cross-link may also slide. This is in contrast with DLA models where particles are completely immobilized after first contact. We have checked that the depth of the quench does not change the structure or dynamics and obtain indistinguishable results with $\varepsilon_{LJ} = 20kT$, $40kT$, and $80kT$.

Another issue is the role of corrugation. In Fig. 1, we show a cartoon of the LJ and WCA beads spaced at a distance a. If $a/\sigma \approx 1$, the energy landscape is corrugated and there are large barriers to sliding that scale with the bond strength. Even if two parallel LJ rods are in contact, one would need to overcome a barrier to slide them into the global energy minimum with perfect overlap. The corrugation acts like an effective friction between the rods.[16] On one hand, one could consider it a discretization artifact. On the other hand, real surface interactions could have some associated static friction. For $\varepsilon = 10kT$ and $L = 20\sigma$, the choice of $a = 0.4\sigma$: (i) enforces the "athermal" condition that a contact, once formed, will never be broken and (ii) gives a small enough corrugation that contacting rods will eventually slide into complete overlap.

Fig. 2a shows a configuration with low corrugation and uniform attraction. This system shows a tendency for bundling in the absence of explicit patchiness. Rods tend to come into complete overlap. We have checked that for $L = 20\sigma$, $\varepsilon = 10kT$ for larger bead spacings the corrugation prohibits the rods from sliding (not shown). For $a = \sigma$, one forms well developed rigid networks with little bundling even with nominally uniform attraction.

We perform all simulations using LAMMPS.[90] LAMMPS has built-in facilities for efficiently grouping particles into rigid bodies and integrating the equations of motion subject to the rigid body constraints. We used periodic boundary conditions with cubic simulation cells of length $L_{cell} = 3L_{rod} = 60\sigma$. We initiate the runs by equilibrating a hard-rod fluid and then turn on the attractive interactions at $t = 0$. Each run lasts for $t_{max} \approx 5 \times 10^4 \tau$
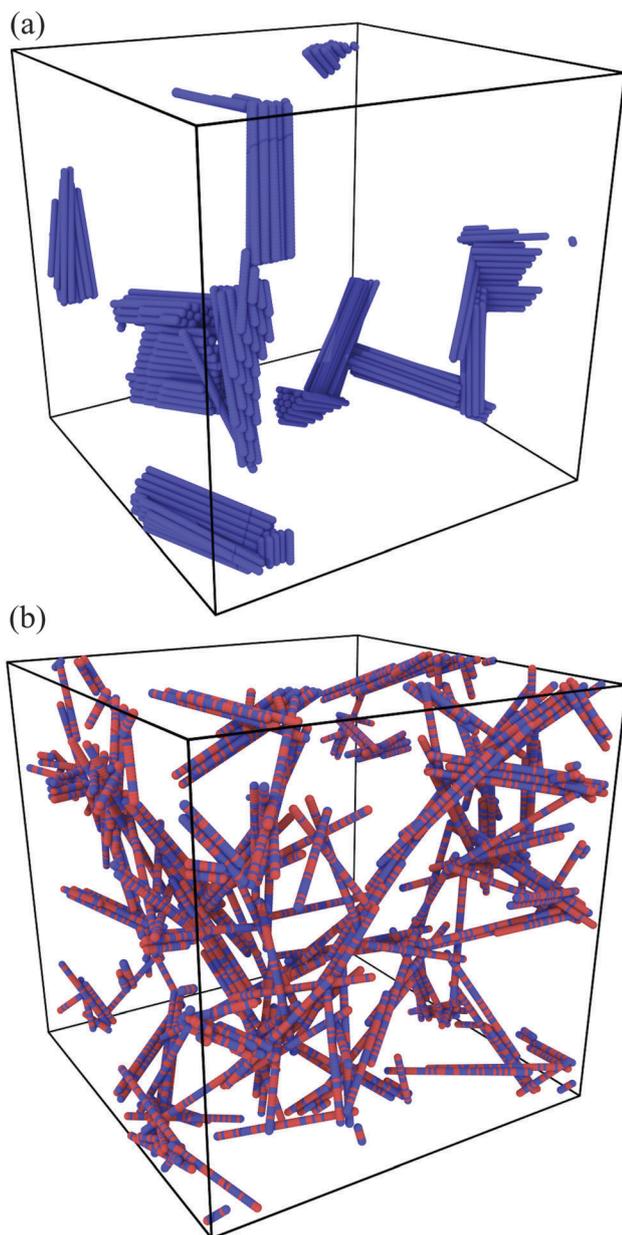
Fig. 2 (a) Typical uniform (non-patchy), low corrugation ($a = 0.4\sigma$) configuration at long time. (b) Typical patchy (50% functionalized surface) low corrugation ($a = 0.4\sigma$) configuration at long time. The uniform system forms disconnected clusters with fluid-like dynamics. The patchy system forms a rigid, spanning network with finite shear modulus and yield stress. Rods which are uniform but with stronger corrugation ($a = \sigma$) not shown may also form rigid, spanning structures with solid-like dynamics.

and requires about one week of running time per system on one core of a modern computing cluster. We perform multiple independent simulations (typically 8) for each set of parameters to improve statistics.

We define the static virial, $\Sigma_{i\alpha\beta}$, associated with each rod *via* a straightforward generalization of the Irving–Kirkwood expression.[91]

$$\Sigma_{i\alpha\beta} = \frac{\partial \phi_i}{\partial \varepsilon_{\alpha\beta}} = -\sum_{j \neq i} F_{ij\alpha} r_{ij\beta} \qquad (1)$$

where: (i) ϕ_i is the potential energy of the *i*-th rod; (ii) $F_{ij\alpha} = -\frac{\partial \phi_{ij}}{\partial r_{ij\alpha}}$ is the net force rod *i* exerts on rod *j*, and (iii) $r_{ij\beta}$ is the separation between the centers of rod *i* and rod *j*. Note that since the net force on any bead is a pairwise sum over neighboring beads, the net force on any rod can also be considered a pairwise sum over neighboring rods. The total static virial, $\Sigma_{\alpha\beta} = \sum_i \Sigma_{i\alpha\beta}$, then gives the total derivative of the potential energy with respect to a homogeneous strain.

3 Structure and dynamics during gelation

3.1 Structure

In Fig. 3, we show the structure factor, $S(q)$, at various times during gelation for $f = 40\%$ (typical of a rigid, strong network) and $f = 80\%$ (approaching the bundling transition and rigidity loss) at three different times: $t = 5 \times 10^2 \tau$, $t = 5 \times 10^3 \tau$, and $t = 5 \times 10^4 \tau$. To compute the scattering intensity, we simply take the individual beads making up the rod to be point scatterers.

$$I(\vec{q}) = S(\vec{q}) = \left| \frac{1}{N} \sum_i \exp(i\vec{q} \cdot \vec{r}_i) \right|^2$$

where $\vec{r}_i$ is the position of bead *i* and *N* is the total number of beads in the system. $S(q)$ is then an isotropic average of $S(\vec{q})$. Note that we non-dimensionalize the wave vector by the rod diameter rather than the rod length.§ Recall that we start from an equilibrated hard-rod state. For spatially uncorrelated rods with uniform uncorrelated orientation, $S \sim q^{-1}$. Our data are consistent with this behavior in the initial equilibrated hard-rod state, but quickly depart from this as gelation proceeds. The departure is largest and most rapid for the systems with the highest *f* on the verge of bundling.

For any *f*, the structure has long-lived evolution. It is still evolving at the longest times studied with systematically increasing power at the smallest wavevector for all *f*. In Fig. 4, we plot $S(q)$ at long time for various *f*. For all *f*, the intermediate regime for *q* between the bead scale $q/2\pi \approx 1/\sigma$ and the rod scale, $q/2\pi \approx 1/L$, $S(q)$ is significantly steeper than q^{-1}. For $f < 60\%$, the spectra are difficult to distinguish from each other. The slope is somewhere between -1 and -2 and is roughly constant over the whole range of $q\sigma/2\pi$. For $f \geq 70\%$ For large *f*, the slope is steeper than -2 for $1 \times 10^{-1} \leq q\sigma/2\pi \leq 5 \times 10^{-1}$.

One might expect one of the several idealized behaviors for rod networks.[92,93] On very general grounds, at wavelengths longer than the longest wavelength over which structure is correlated, $S(q)$ should become flat. At shorter wavelength, one would expect the structure to look different in the cases of rigid networks and disconnected clusters.

The idealized case of homogeneous rigid rod networks consists of a single characteristic "pore size", ξ_{pore}. ξ_{pore} is envisioned to be less than the rod length, *L*, and it decreases with increasing volume fraction as the pore space closes.

§ For $L = 20\sigma$, $q\sigma/2\pi = 1/20$ corresponds to the rod length.
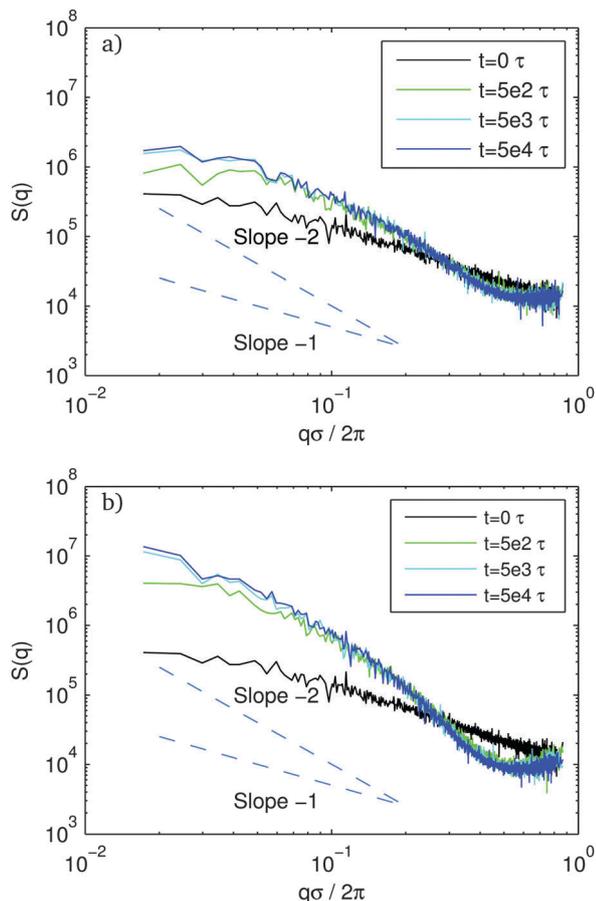
Fig. 3 Structure factor, $S(q)$, for rod networks at various waiting time: $t = 0$ (black), $5 \times 10^2\tau$ (green), $5 \times 10^3\tau$ (cyan), $5 \times 10^4\tau$ (blue). Fraction, f, of attractive sites: (a) 40%, (b) 80%. The blue dashed lines are $S \sim q^{-1}$ and $S \sim q^{-2}$ for reference.
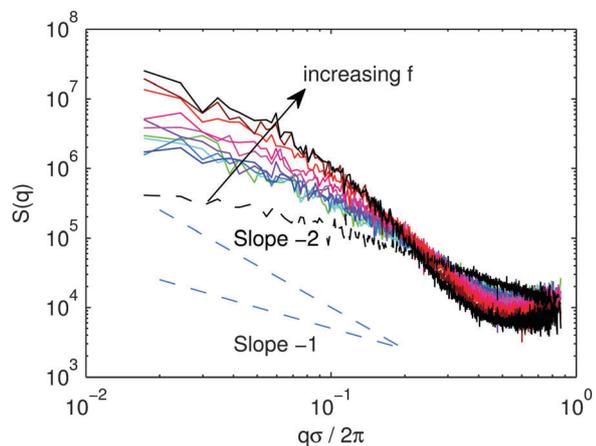

Fig. 4 Structure factor, $S(q)$, for rod networks at various f for $t_w = 5 \times 10^4\tau$.

At high q where $q\xi_{pore} \geq 2\pi$, the structure factor displays the characteristic shape for the rigid uncorrelated rods, $S \sim q^{-1}$. At longer wavelength, $q\xi_{pore} \leq 2\pi$, the density becomes uncorrelated and $S \sim$ const. Fractal networks[55,92,94] present an alternative picture where there is no characteristic pore size and $S(q)$

follows a power law with a non-trivial exponent out to the largest lengths.

At densities too low for gel formation, and for $\varepsilon \gg kT$, disconnected clusters are thought to form *via* DLA. In the idealized case of fractal clusters, $S(q)$ for $qL \ll 1$ scales like $S \sim q^{-D}$ where D is the fractal dimension of the cluster,[88] as in the case of diffusion limited cluster formation of spheres. Beyond the characteristic cluster size $q\xi_{cluster} < 2\pi$, the density becomes uncorrelated and S_{const}. The fractal dimension depends on the aspect ratio. Clusters of rods formed *via* DLA with an aspect ratio near those studied here have $D \approx 2.1$.[88]

At late times, for all f, we never observe a clear plateau in $S(q)$ or any other characteristic scale indicating any sort of "pore" at shorter wavelength than the rod length. The $S(q)$ curve of the more highly bundled systems at high f starts off with a high slope in the $qL \approx 2\pi$ regime and starts to slightly flatten at the smallest q, but no clear plateau emerges for the system sizes studied here. The more homogeneous networks have a roughly constant slope between 1 and 2 throughout most of the range, and we can essentially rule out the development of a characteristic pore scale at nearby q. Our data for the more regular networks at low f could be consistent with the fractal network models, while the bundled networks at high f might be more in line with the homogeneous rod network picture with $\xi_{pore} \geq L$. The emergence of a characteristic scale could be a signature for the impending network collapse. However, one should be careful in interpreting this characteristic scale as a pore size; it might be better to think of it as the characteristic scale of the bundles which form in the disconnected state.

3.2 Dynamics

In Fig. 5, we plot the energy as a function of time for the ensembles with various f. The potential energy, U, is normalized by both ε_{LJ} and the total number of attractive beads, n, at the given f. Recall, all simulations here were for a binding energy of $\varepsilon_{LJ} = 10kT$. Because of the strong binding, the energy almost always decreases as more and more links form. Because of these essentially athermal dynamics, the normalized energy serves as a simple proxy for the total number of attractive contacts.
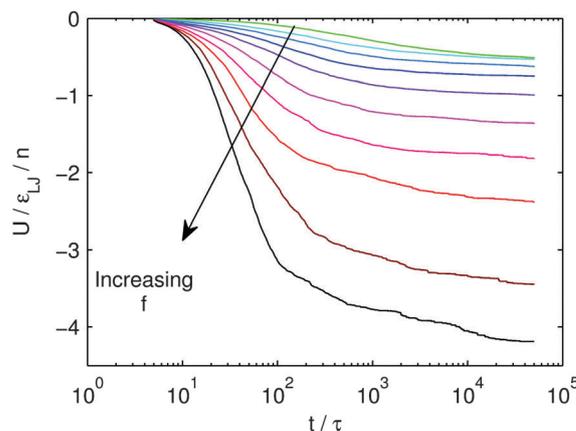

Fig. 5 Energy *vs.* time for various f. The total energy is normalized by the total number of attractive sites for any f.

Systems which have a value of more than −1 have fewer than one bond on average for each potential binding site. Systems that have a value of less than −4 have more than four bonds on average for each potential binding site. This is a manifestation of the thick bundles observed for the uniform rods in Fig. 2.

Note that the energy is still relaxing at the longest times simulated, corresponding to $t = 5 \times 10^4\tau$. The slow relaxation is reminiscent of glassy relaxation and logarithmic compaction in granular tapping experiments.[95,96] As the network becomes increasingly slow and rigid, it becomes harder and harder to find new crosslinking sites. Furthermore, in the systems with relatively high f, there are large, discrete energy drops. In real space, these events correspond to large restructuring events where branches of the network effectively merge into thicker ones.

In Fig. 6, we plot the mean squared displacement (MSD) of rod centers at various waiting time, t_w for $f = 10\%$ and $f = 40\%$. Fig. 7 shows the same MSD plots for $f = 80\%$ and $f = 90\%$. The heavy dashed line in the upper corner represents free diffusion of a single bead. For $f = 10\%$, for the very youngest systems, the MSD curves start in a diffusive regime and show a flattening as clusters start to form. Even for the oldest systems, the curves remain subdiffusive at long time and never show any clear solid-like plateau at intermediate time. Despite the lack of a plateau in the MSD curve, as we show below, a rigid backbone has already developed, and the system does have a well defined shear modulus.

At a slightly higher f, the MSD starts to develop a proper plateau, at intermediate times, characteristic of a solid. At long times, the MSD values depart from the plateau with a pronounced sub-diffusive slope. This long time behavior is much like the lower f systems which do not develop any plateau. As we show below, we find little difference in the non-linear mechanical response when comparing the systems with and without a plateau.

Above about $f = 50\%$, a new trend emerges. The dynamics becomes bursty for old systems. Consider the system with $f = 80\%$. The oldest sample shows an initial plateau. The plateau is lower than the $f = 40\%$ system indicating increased stiffness at intermediate times. But the $f = 80\%$ system shows a sudden jump by almost two orders of magnitude at $t - t_w \approx 10^4\tau$. In real space these events correspond to large discrete reconfigurations where large branches of the network reorient and merge with others.¶ These bursts are direct manifestations of the large energy drops observed above in Fig. 5. As f increases, the height of the initial plateau is roughly constant. However, the jumps corresponding to shifts in the plateau height become bigger in magnitude indicating larger events.

Finally at a binding fraction above $f = 90\%$, there is no longer any solid-like MSD plateau. In real space, there is complete bundling of rods and collapse of the network. The loading curves we present below indicate that, in many – but not all – of the members of the ensemble, the structure is no longer rigid and has no low frequency storage modulus. These members of the ensemble with disconnected clusters and no rigid backbone give rise to essentially diffusive behavior with a diffusion coefficient roughly 3 orders of magnitude below a free rod. We presume that if
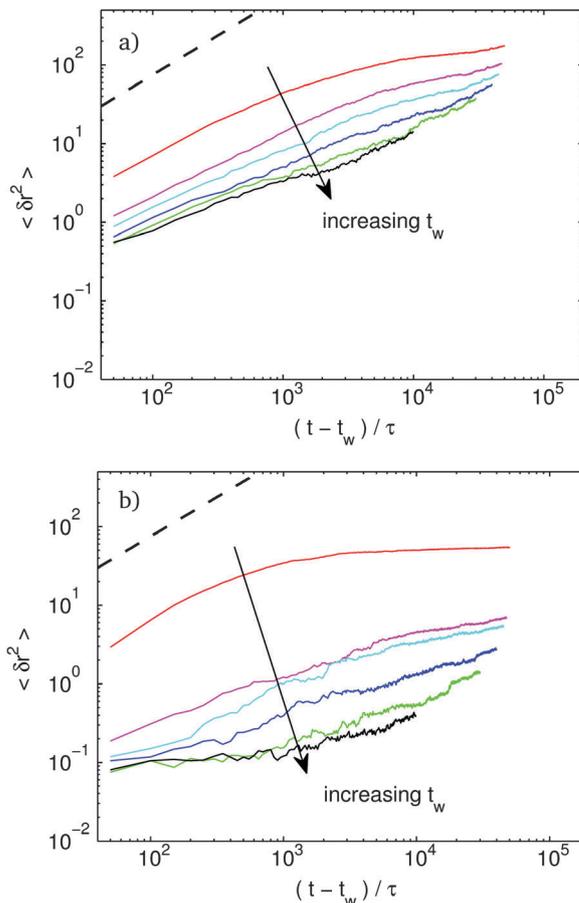
¶ See videos in the ESI.†

Fig. 6 Mean squared displacement vs. time for various waiting time, t_w. Red: $t_w = 5 \times 10^1\tau$, magenta: $t_w = 2.5 \times 10^3\tau$, cyan: $t_w = 5 \times 10^3\tau$, blue: $t_w = 1 \times 10^4\tau$, green: $t_w = 2 \times 10^4\tau$, black: $t_w = 4 \times 10^4\tau$. Attractive site coverage, (a) $f = 10\%$, (b) $f = 40\%$. The dashed line is the free-bead diffusion curve, $\delta r^2 = (t - t_w)/\tau$, for reference.

we were able to run the simulation for a longer time, the diffusion coefficient would go down even further as the disconnected clusters continue to coarsen. We conjecture that once the characteristic bundle size reaches the rod length, the bundles would start to aggregate into clumps much like in conventional DLA of spherical particles. Checking this conjecture would, of course, require simulations at significantly longer lengthscales.

4 Non-linear mechanical response

In Fig. 8, we plot the axial stress vs. axial strain (in extension) for various f. The networks are aged for the full $t = 5 \times 10^4\tau$ and then relaxed with a short zero temperature simulation to find a nearby mechanical equilibrium state without allowing further aging of the network. The networks are then loaded in an athermal, quasi static protocol: the cell is slowly deformed under a zero temperature Brownian dynamics. We deform the systems along one axis of the box, x, such that the length of the box on that axis, $L_x = (1 + \varepsilon)L_{x0}$, where L_{x0} is its initial length and ε is the axial strain. Note that in this loading protocol, we neither preserve volume nor control the loads transverse to the

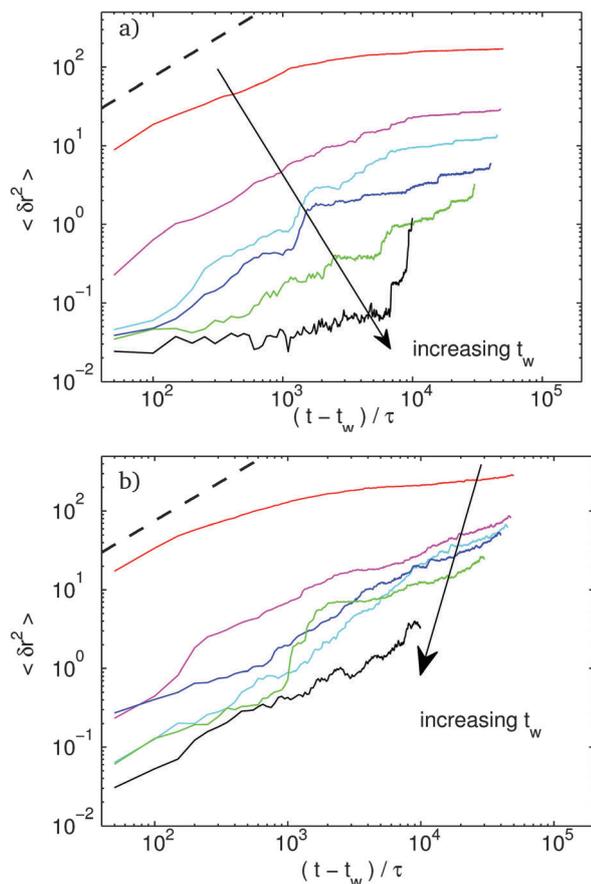Fig. 7 The same as Fig. 6 for (a) f = 80%, (b) f = 90%.

Fig. 9 Axial stress vs. strain for different systems in an ensemble with (a) f = 20%, (b) f = 80%. Blue-dashed curve is the average of 8 systems shown in Fig. 8.
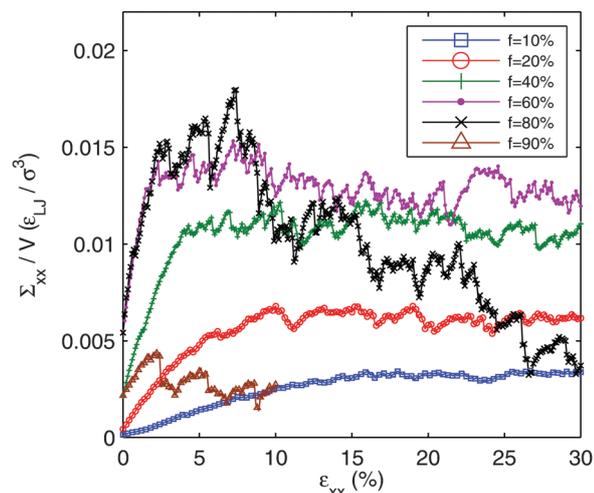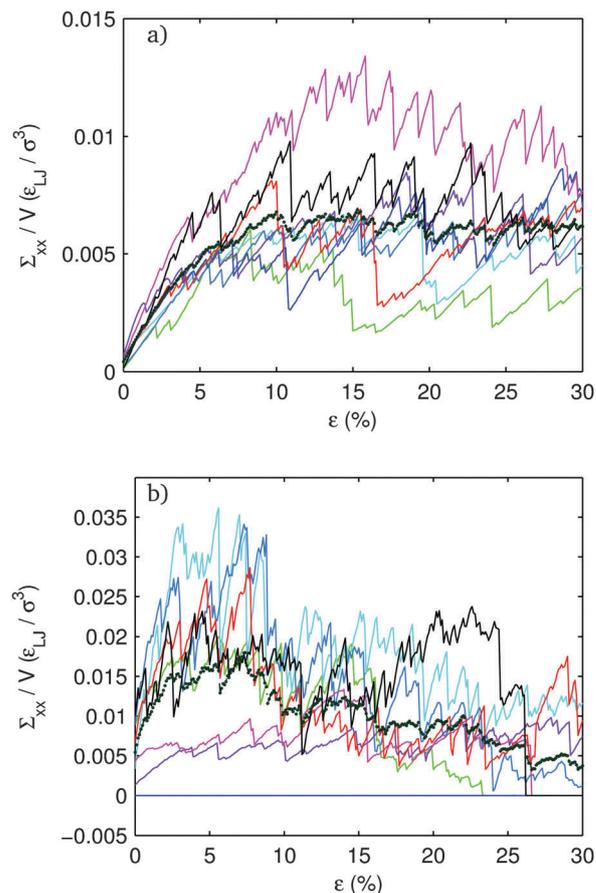

Fig. 8 Axial stress vs. strain for various f (20% through 90%). Stress is calculated and shown by dividing conjugate static virial (Σ_{xx}) by the volume (V). Deformation is axial extension along the 'x'-axis, such that $\varepsilon_{yy} = \varepsilon_{zz} = 0$.

extension direction. Eight independent runs are conducted at each f to improve statistics.

At all f, studied here, a rigid network forms in at least some of the members of the ensemble. In Fig. 9, we show the full set of 8 systems for f = 20% and f = 80%. After the initial gelation,

all the systems acquire a residual tensile stress. Upon deformation the tensile stress increases linearly, with discrete drops at well define strains. These events are reminiscent of the elementary plastic yielding events observed in amorphous solids.[97] Along any one of the linear ramps, the deformation is completely reversible. After (and only after) any of the load drops, the deformation becomes irreversible, and the system does not revert to previous configurations upon unloading.

The loading curves have a remarkable dependence on f. For the lowest f there is a slight strain stiffening. The slope of the loading curve goes up with strain. This is similar to what is seen in spring networks[98] where the imposed shearing activates tension in branches of the network in initially unloaded, floppy, strands. For f = 10%, the stress increases essentially monotonically throughout the range of strain. In this sense, it can be considered a tough, ductile material.

As f increases, the initial tensile stress and slope increase. For f = 20%, the stress also reaches a long-time plateau. However, it reaches this plateau, by about 10% strain, much more quickly than the f = 10% system. The f = 40% is qualitatively the same as f = 20%, but with an even sharper crossover to the yield stress plateau at an even smaller strain of about 4%. By f = 60%, the loading curves start to change qualitatively. The stress no longer monotonically increases. The f = 60% loading curve

exhibits a peak stress between about 5% and 10% strain with a slight softening beyond that. The $f = 80\%$ system shows a peak stress of roughly the same height and at roughly the same strain as the $f = 60\%$ system, but with a dramatically larger softening.

Looking at the individual members of an ensemble, shown in Fig. 9, gives more insight. At $f = 20\%$ all of the systems in the ensemble are rigid. The fluctuations about the average stress in steady shear are on the order of the average. The system with the largest peak stress shows some softening upon approaching to the steady state, but none of the others do. None of the systems show any tendency for softening in the steady regime and all systems remain rigid out to 30% strain.

At $f = 80\%$ the picture is qualitatively different. There are much more dramatic fluctuations within the ensemble. One of the 8 systems is not even rigid. Two of the rigid systems start well below the ensemble average stress and are much less stiff. These two systems do not show very much softening during shear. In contrast, those systems that lie above the ensemble average show a very pronounced softening after the peak stress. By the end of the 30% strain interval, three systems, in addition to the one which failed to percolate initially, have completely failed. The picture which emerges is that, although these high f systems are stiffer and stronger on average, they are much more fragile and have a significantly lower strain threshold before rigidity breaks down and the stress drops to zero.

The initial linear ramps in the loading curves allow us to define an elastic modulus. In Fig. 10, we plot the elastic modulus for various f. The error bars represent the variance of the modulus across the members of the ensemble. At low f, the modulus and fluctuations increase with increasing f. Finally, at 80%, the modulus reaches a maximum and drops dramatically to zero at larger f. This peak value of the modulus occurs at roughly the same value of f where we first observe the catastrophic softening behavior in steady shear.

In Fig. 11 and 12, we show orthographic projection in the x–y and x–z planes of the rods during loading for $f = 20\%$ (below optimal) and $f = 80\%$ (above optimal) for the initial relaxed state, after loading to 15% and 30%. The rods are colored according to Σ_{xx}, the component of the static virial conjugate
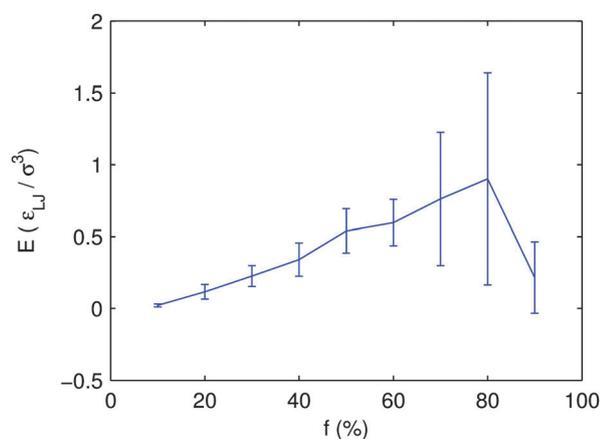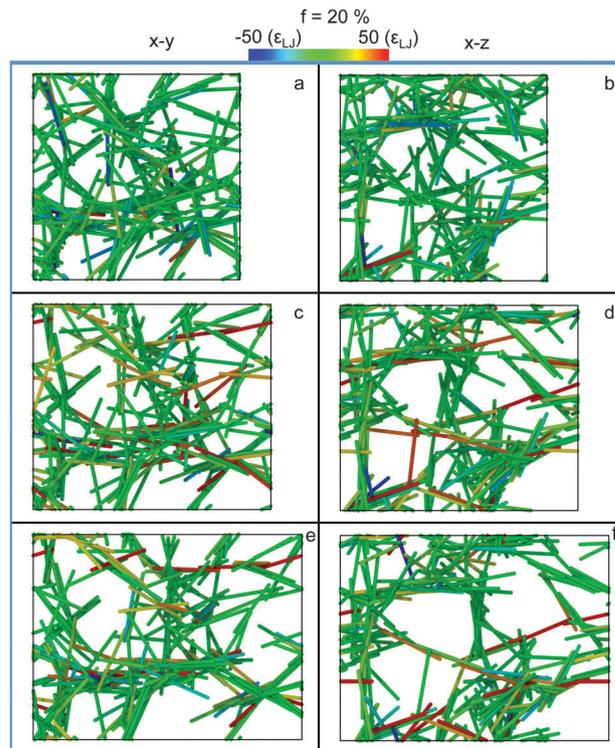

Fig. 11 Orthographic projection in the xy and xz planes of: (a and b) unstrained, (c and d) 15% and (e and f) 30% strained configuration for $f = 20\%$. The extension axis, x, is horizontal. Rods are colored according to the their contribution to the total Virial in the stretching direction, Σ_{xx}. Red indicates tensile and blue compressive stresses.

to the applied axial strain ε_{xx}. Red indicates tension, blue compression, and green unstressed rods.

There are dramatic differences between the two systems. The $f = 20\%$ system is much more homogeneous with a well dispersed, network which is globally isotropic. The red rods supporting the large tensile loads at 30% strain tend to be aligned along the extension axis. These same rods started in the unsheared network with stresses that were smaller in magnitude but still tensile in nature and with orientations which were predominantly along the loading axis.

The $f = 80\%$ system is very different. In the unsheared state, it shows significant bundling of rods (discussed above) and a few thick network branches composed of these bundles. Much of the network undergoes very little reorientation under shear while only those branches oriented along the extension axis undergo elongation. One would naively guess that the system should be stronger because of the increased number of inter-rod binding sites. However, it is actually weaker since there are fewer network branches to support the applied load. The resulting deformation is much less homogeneous.

In Fig. 13 and 14, we show the distribution of the angle-cosines (for the angle of the rod with respect to the extension axis) at the initial unstrained configuration and for a strain of 30% along with the nematic order parameter, $S = \langle 3\cos^2(\theta) - 1 \rangle / 2$. For $f = 20\%$, S increases smoothly and essentially monotonically throughout the range, starting from around $S = 0$ and ending at around $S = 7\%$.
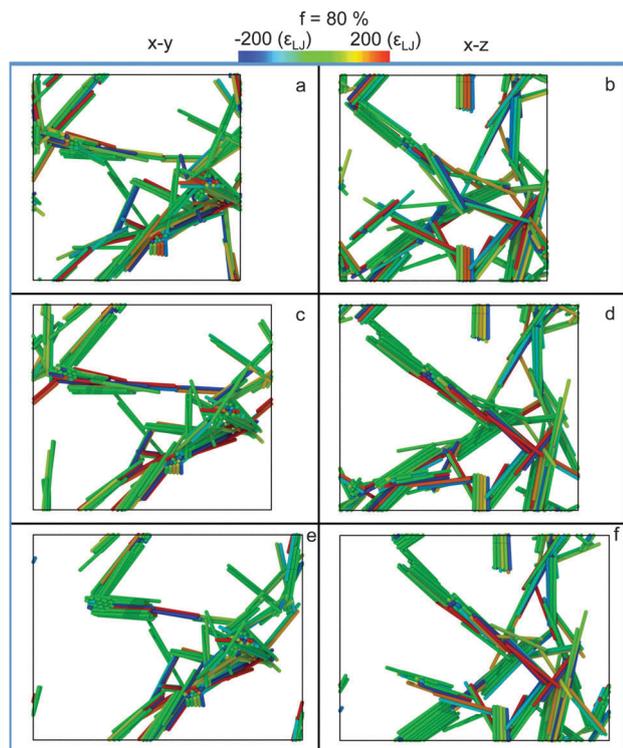

Fig. 10 Elastic modulus vs. f.

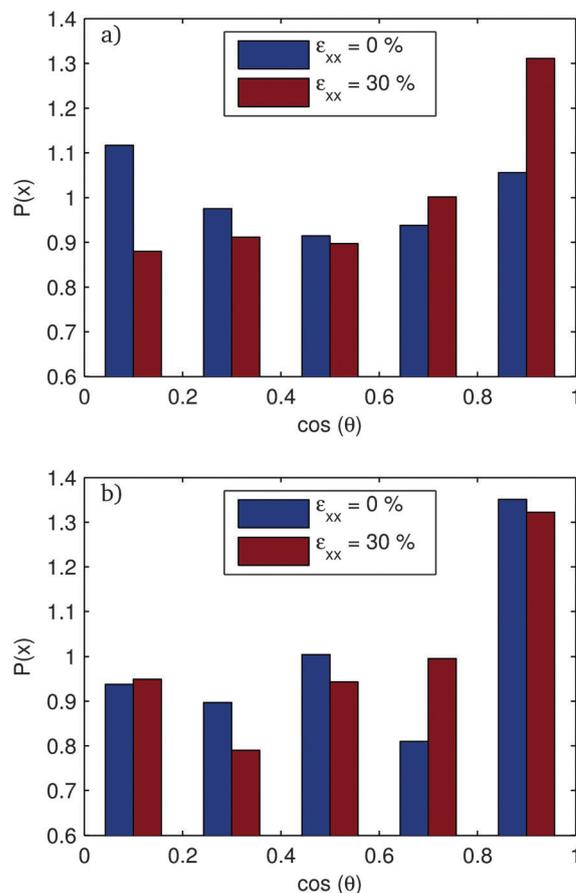Fig. 12 The same as Fig. 11, but for f = 80%.

Fig. 13 Distribution of orientation $x = \cos(\theta_x)$ at a strain of 0% and 30% for the systems with surface fraction (a) 20% and (b) 80%. $\cos(\theta_x)$ is the cosine of the angle the rod makes with the extensional axis.

The f = 80% system has large fluctuations in S. The unsheared systems show large fluctuations within the ensemble. This is due to the perfect orientational ordering within bundles. Each bundle has a given orientation. There are fewer independent orientations over which to average, and the orientation distribution is subject to small number statistics. S values have strong member-to-member fluctuations within the ensemble.

We can attempt to understand the predominant value of the slope of the S vs. ε curves using a simple model where any rod is just advected with the homogeneous, affine deformation. If we assume that the component of the velocity of the tip of a rod perpendicular to its length is equal to the homogeneous affine flow field at that point, we get:

$$v_\theta = -\dot{\varepsilon}L\cos(\theta)\sin(\theta) \tag{2}$$

Then we have:

$$v_x = \frac{d}{dt}x = \dot{\varepsilon}x(1-x^2) \tag{3}$$

where x, as usual, is the cosine of the angle the rod makes with the extension axis. We assume that the whole orientation distribution, P, is simply advected:

$$\frac{\partial P}{\partial t} = -\frac{\partial}{\partial x}(v_x P) \tag{4}$$

We can then write an equation for the second moment of the distribution:

$$\frac{d\langle x^2\rangle}{dt} = -\int_0^1 x^2\frac{\partial}{\partial x}(v_x P)dx \tag{5}$$

Assuming we start with an isotropic distribution P = 1, we get:

$$\frac{d\langle x^2\rangle}{dt} = -\dot{\varepsilon}\int_0^1 x^2(1-3x^2)dx = \frac{4}{15}\dot{\varepsilon} \tag{6}$$

and then

$$\frac{dS}{d\varepsilon} = \frac{3}{2}\frac{d\langle x^2\rangle}{dt}\frac{1}{\dot{\varepsilon}} = \frac{2}{5}. \tag{7}$$

We see from Fig. 14 that the f = 20% system has a distribution of initial slopes, $\frac{dS}{d\varepsilon}$, whose average is 0.37, just slightly less than 2/5. The initial values of S show some scatter, and so do the slopes, but all systems within the ensemble have their rods re-oriented toward the extension axis. The basic picture which emerges is that, for the well connected networks, the rod orientations essentially follow the homogeneous affine flow.

The f = 80% ensemble shows dramatically different behavior. Within the ensemble, there is a broad distribution of initial values of S due to the poor counting statistics associated with the relatively few independently oriented thick network strands. Many systems show strongly non-affine motion with hardly any reorientation of rods at all. In these systems, a small number of thick trunks of the load bearing network extend in response
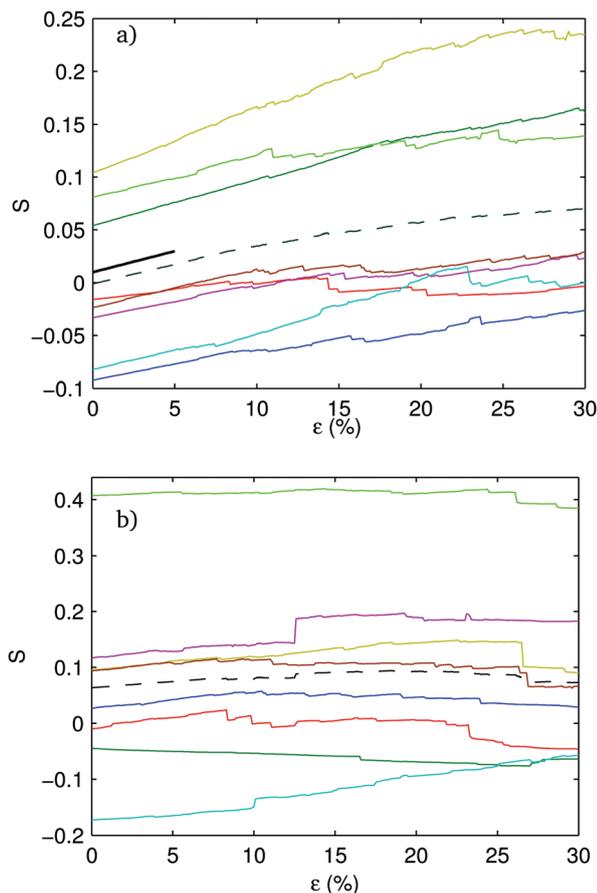
Fig. 14 Nematic order parameter, S, as a function of ε, for the systems with surface fraction (a) 20% and (b) 80%. The black solid line shows the slope of Nematic order parameter *versus* ε for rods deforming affinely with the extension flow.

to the strain and eventually disconnect without appreciable reorientation of rods. This suggests that strongly non-affine behavior of $S(\varepsilon)$ might be taken as indicative of poor mechanical properties and potential catastrophic failure after peak load.

5 Conclusions

We presented the results of a simple model for aggregation and mechanical response of rod-like particles, and showed that the networks that form depend on the details of the inter rod interactions. If the rods were uniformly attractive with no irregularity in the surface interactions, disconnected clusters form. In our simple model, the rods were composed of beads with a fraction, f, which were able to stick to other beads of the attractive variety on other rods. We studied structure and dynamics during gelation, and we then subjected the well-aged gels to athermal quasi-static straining to probe the mechanical robustness of the networks. We showed that intermediate values of f gave optimal mechanical properties (enhanced modulus, yield stress, and total strain to failure) and dramatically different spatial structure and gelation

dynamics than the either low or high values of f. In this sense, these results may be seen as providing guiding principles for tailoring surface interactions between rods for optimal structural, mechanical, or electronic properties.

The dynamical measurements during gelation are most directly comparable to experiments by Chen *et al.* on NaDDBS-stabilized single walled CNTs suspended in water.[25] Chen *et al.* used tracer diffusion and found a short-time diffusion coefficient of roughly 1 μm^2 s^{-1} after aging for t_w = 10 minutes, which was essentially a plateau in the MSD at a value of about 2×10^{-3} μm^2 after t_w = 3 hours. The height of the plateau was still decreasing at that time. There are striking similarities to the MSD curves for our systems in the intermediate range of f. In particular, the value of the MSD at the onset of the plateau is reduced by about two orders of magnitude from the early, $t_w \rightarrow 0$ limit, and this is consistent with the data from our model.

The work presented here should be considered a first step toward modeling the aggregation of nominally-stabilized suspensions of rod-like particles. It opens up many directions for future work. (i) As we have shown above, the structure shows no characteristic length scale for the optimal systems at intermediate f. Does one emerge just beyond the limited system sizes studied here as in the conventional homogeneous rod network picture,[99] or does one have fractal structure out to the longest lengths?[55,92,94] Larger simulations are necessary. (ii) In this study we have worked at a constant aspect ratio and volume fraction well above the threshold for gel formation. One would guess that the critical volume fraction, ϕ, for gel formation would be strongly dependent on f, with the more bundled networks forming at higher f requiring higher ϕ to gel. The ϕ dependence should be checked explicitly. (iii) The strong system-to-system fluctuations within the ensemble at high f (a few systems have zero modulus at f = 80%, while a few systems have finite modulus at f = 90%) would indicate strong finite size effects. Is there a phase transition underlying these effects, and would there be a sharp transition f_c with $f_c < 1$ beyond which no systems gel in the infinite size limit? In analogy with rigidity percolation or jamming, one could plot the fraction of rigid systems in the ensemble as a function of f for various system sizes. One would expect, in general, a sigmoidal shape where both the width and the location of the transition would depend on system size. A finite size analysis is called for. (iv) There should be a lower bound on f, below which there are too few cross linking sites to form a network. Can we use arguments from rigidity percolation to understand how the modulus in the virgin, unstrained systems depends on the number of cross linking sites and/or the number of active cross links formed after gelation? (iv) We have shown that the systems at intermediate f are extremely robust mechanically. They can be strained to 30% at essentially constant stress with little hardening or softening. In applications, such as flexible electronics,[100,101] it is crucial to understand the ultimate strain the network can sustain before it falls apart, and it would be very interesting to continue the simulations at intermediate f out to larger strains and ultimate failure.

Acknowledgements

References

1 V. M. Cepak and C. R. Martin, *J. Phys. Chem. B*, 1998, **102**, 9985–9990.

2 M. J. A. Hore and R. J. Composto, *ACS Nano*, 2010, **4**, 6941–6949.

3 J. M. Romo-Herrera, R. A. Alvarez-Puebla and L. M. Liz-Marzan, *Nanoscale*, 2011, **3**, 1304–1315.

4 J. Vonnemann, N. Beziere, C. Böttcher, S. B. Riese, C. Kuehne, J. Dernedde, K. Licha, C. von Schacky, Y. Kosanke, M. Kimm, R. Meier, V. Ntziachristos and R. Haag, *Theranostics*, 2014, **4**, 629–641.

5 R. M. Erb, R. Libanori, N. Rothfuchs and a. R. Studart, *Science*, 2012, **335**, 199–204.

6 E. J. Garboczi, K. A. Snyder, J. F. Douglas and M. F. Thorpe, *Phys. Rev. E: Stat. Phys., Plasmas, Fluids, Relat. Interdiscip. Top.*, 1995, **52**, 819–828.

7 M. Adams, Z. Dogic, S. L. Keller and S. Fraden, *Nature*, 1998, **393**, 349–352.

8 P. Terech, L. Chazeau and J. Y. Cavaille, *Macromolecules*, 1999, **32**, 1872–1875.

9 M. M. D. Lima and R. Borsali, *Macromol. Rapid Commun.*, 2004, **25**, 771–787.

10 F. M. Du, R. C. Scogna, W. Zhou, S. Brand, J. E. Fischer and K. I. Winey, *Macromolecules*, 2004, **37**, 9048–9055.

11 C. A. Dyke and J. M. Tour, *J. Phys. Chem. A*, 2004, **108**, 11151–11159.

12 M. Moniruzzaman and K. I. Winey, *Macromolecules*, 2006, **39**, 5194–5205.

13 N. G. Sahoo, S. Rana, J. W. Cho, L. Li and S. H. Chan, *Prog. Polym. Sci.*, 2010, **35**, 837–867.

14 A. V. Kyrylyuk and P. van der Schoot, *Proc. Natl. Acad. Sci. U. S. A.*, 2008, **105**, 8221–8226.

15 M. A. Zirnsak, D. V. Boger and V. Tirtaatmadja, *J. Rheol.*, 1999, **43**, 627–650.

16 C. F. Schmid, L. H. Switzer and D. J. Klingenberg, *J. Rheol.*, 2000, **44**, 781–809.

17 K. Dawson, G. Foffi, M. Fuchs, W. Gotze, F. Sciortino, M. Sperl, P. Tartaglia, T. Voigtmann and E. Zaccarelli, *Phys. Rev. E: Stat., Nonlinear, Soft Matter Phys.*, 2001, **63**, 011401.

18 F. Sciortino, S. Mossa, E. Zaccarelli and P. Tartaglia, *Phys. Rev. Lett.*, 2004, **93**, 5–8.

19 P. J. Lu, E. Zaccarelli, F. Ciulla, A. B. Schofield, F. Sciortino and D. A. Weitz, *Nature*, 2008, **453**, 499–U4.

20 E. Zaccarelli, *J. Phys.: Condens. Matter*, 2007, **19**, 323101.

21 M. P. B. van Bruggen, J. K. G. Dhont and H. N. W. Lekkerkerker, *Macromolecules*, 1999, **32**, 2256–2264.

22 X. Fan, N. Phan-Thien and R. Zheng, *J. Non-Newtonian Fluid Mech.*, 1998, **74**, 113–135.

23 C. J. Petrie, *J. Non-Newtonian Fluid Mech.*, 1999, **87**, 369–402.

24 Y.-G. Tao, W. den Otter and W. Briels, *Phys. Rev. Lett.*, 2005, **95**, 237802.

25 A. Mohraz and M. J. Solomon, *J. Colloid Interface Sci.*, 2006, **300**, 155–162.

26 D. T. N. Chen, K. Chen, L. A. Hough, M. F. Islam and A. G. Yodh, *Macromolecules*, 2010, **43**, 2048–2053.

27 K. Shikinaka, K. Kaneda, S. Mori, T. Maki, H. Masunaga, Y. Osada and K. Shigehara, *Small*, 2014, **10**, 1813–1820.

28 S. Lin-Gibson, J. Pathak, E. Grulke, H. Wang and E. Hobbie, *Phys. Rev. Lett.*, 2004, **92**, 048302.

29 E. Hobbie and D. Fry, *Phys. Rev. Lett.*, 2006, **97**, 036101.

30 R. Bandyopadhyaya, E. Nativ-Roth, O. Regev and R. Yerushalmi-Rozen, *Nano Lett.*, 2002, **2**, 25–28.

31 M. F. Islam, E. Rojas, D. M. Bergey, A. T. Johnson and A. G. Yodh, *Nano Lett.*, 2003, **3**, 269–273.

32 O. Matarredona, H. Rhoads, Z. R. Li, J. H. Harwell, L. Balzano and D. E. Resasco, *J. Phys. Chem. B*, 2003, **107**, 13357–13367.

33 O. Matarredona, H. Rhoads, Z. R. Li, J. H. Harwell, L. Balzano and D. E. Resasco, *J. Phys. Chem. B*, 2003, **107**, 13357–13367.

34 E. K. Hobbie and D. J. Fry, *J. Chem. Phys.*, 2007, **126**, 124907.

35 M. D. Clark, S. Subramanian and R. Krishnamoorti, *J. Colloid Interface Sci.*, 2011, **354**, 144–151.

36 E. K. Hobbie, *Rheol. Acta*, 2010, **49**, 323–334.

37 A. J. Blanch, C. E. Lenehan and J. S. Quinton, *J. Phys. Chem. B*, 2010, **114**, 9805–9811.

38 S. H. Qin, D. Q. Qin, W. T. Ford, D. E. Resasco and J. E. Herrera, *Macromolecules*, 2004, **37**, 752–757.

39 M. J. O'Connell, P. Boul, L. M. Ericson, C. Huffman, Y. Wang, E. Haroz, C. Kuper, J. Tour, K. D. Ausman and R. E. Smalley, *Chem. Phys. Lett.*, 2001, **342**, 265–271.

40 C. Zakri and P. Poulin, *J. Mater. Chem.*, 2006, **16**, 4095–4098.

41 W. Zhou, M. F. Islam, H. Wang, D. L. Ho, A. G. Yodh, K. I. Winey and J. E. Fischer, *Chem. Phys. Lett.*, 2004, **384**, 185–189.

42 D. Fry, B. Langhorst, H. Kim, E. Grulke, H. Wang and E. Hobbie, *Phys. Rev. Lett.*, 2005, **95**, 038304.

43 H. Wang, W. Zhou, D. L. Ho, K. I. Winey, J. E. Fischer, C. J. Glinka and E. K. Hobbie, *Nano Lett.*, 2004, **4**, 1789–1793.

44 N. R. Tummala and A. Striolo, *ACS Nano*, 2009, **3**, 595–602.

45 B. J. Bauer, E. K. Hobbie and M. L. Becker, *Macromolecules*, 2006, **39**, 2637–2642.

46 L. Hough, M. Islam, P. Janmey and A. Yodh, *Phys. Rev. Lett.*, 2004, **93**, 168102.

47 M. O'Connell, P. Boul and L. Ericson, *Chem. Phys.*, 2001, **342**, 265–271.

48 M. Calvaresi, S. Hoefinger and F. Zerbetto, *Chemistry*, 2012, **18**, 4308–4313.

49 L. A. Hough, M. F. Islam, B. Hammouda, A. G. Yodh and P. A. Heiney, *Nano Lett.*, 2006, **6**, 313–317.

50 L. Vaisman, H. D. Wagner and G. Marom, *Adv. Colloid Interface Sci.*, 2006, **128**, 37–46.

51 N. Grossiord, P. van der Schoot, J. Meuldijk and C. E. Koning, *Langmuir*, 2007, **23**, 3646–3653.

52 M. Suttipong, N. R. Tummala, B. Kitiyanan and A. Striolo, *J. Phys. Chem. C*, 2011, **115**, 17286–17296.

53 N. M. Uddin, F. M. Capaldi and B. Farouk, *Comput. Mater. Sci.*, 2012, **53**, 133–144.

54 M. Calvaresi, M. Dallavalle and F. Zerbetto, *Small*, 2009, **5**, 2191–2198.

55 T. Chatterjee, A. Jackson and R. Krishnamoorti, *J. Am. Chem. Soc.*, 2008, **130**, 6934–6935.

56 B. Vigolo, C. Coulon, M. Maugey, C. Zakri and P. Poulin, *Science*, 2005, **309**, 920–923.

57 V. A. Davis, A. N. G. Parra-Vasquez, M. J. Green, P. K. Rai, N. Behabtu, V. Prieto, R. D. Booker, J. Schmidt, E. Kesselman, W. Zhou, H. Fan, W. W. Adams, R. H. Hauge, J. E. Fischer, Y. Cohen, Y. Talmon, R. E. Smalley and M. Pasquali, *Nat. Nanotechnol.*, 2009, **4**, 830–834.

58 M. Calvaresi, S. Hoefinger and F. Zerbetto, *Chemistry*, 2012, **18**, 4308–4313.

59 M. J. Green, A. N. G. Parra-Vasquez, N. Behabtu and M. Pasquali, *J. Chem. Phys.*, 2009, **131**, 1–10.

60 V. A. Davis, L. M. Ericson, A. N. G. Parra-Vasquez, H. Fan, Y. H. Wang, V. Prieto, J. A. Longoria, S. Ramesh, R. K. Saini, C. Kittrell, W. E. Billups, W. W. Adams, R. H. Hauge, R. E. Smalley and M. Pasquali, *Macromolecules*, 2004, **37**, 154–160.

61 F. Huang, R. Rotstein, S. Fraden, K. E. Kasza and N. T. Flynn, *Soft Matter*, 2009, **5**, 2766–2771.

62 A. P. Philipse and A. M. Wierenga, *Langmuir*, 1998, **14**, 49–54.

63 M. P. B. van Bruggen, *Langmuir*, 1998, **14**, 2245–2255.

64 M. P. B. van Bruggen and H. N. W. Lekkerkerker, *Langmuir*, 2002, **18**, 7141–7145.

65 M. van Bruggen, H. Lekkerkerker and J. Dhont, *Phys. Rev. E: Stat. Phys., Plasmas, Fluids, Relat. Interdisc. Top.*, 1997, **56**, 4394–4403.

66 A. Wierenga, A. P. Philipse, H. N. W. Lekkerkerker and D. V. Boger, *Langmuir*, 1998, **14**, 55–65.

67 G. M. H. Wilkins, P. T. Spicer and M. J. Solomon, *Langmuir*, 2009, **25**, 8951–8959.

68 A. S. Karakoti, S. Das, S. Thevuthasan and S. Seal, *Angew. Chem., Int. Ed.*, 2011, **50**, 1980–1994.

69 S. Pierrat, I. Zins, A. Breivogel and C. Sönnichsen, *Nano Lett.*, 2007, **7**, 259–263.

70 R. A. Sperling and W. J. Parak, *Philos. Trans. R. Soc., A*, 2010, **368**, 1333–1383.

71 L. Vigderman, B. P. Khanal and E. R. Zubarev, *Adv. Mater.*, 2012, **24**, 4811–4841.

72 J. Araki, M. Wada, S. Kuga and T. Okano, *Langmuir*, 2000, **16**, 2413–2415.

73 J. Araki, M. Wada and S. Kuga, *Langmuir*, 2001, **17**, 21–27.

74 Y. Boluk, L. Zhao and V. Incani, *Langmuir*, 2012, **28**, 6114–6123.

75 S. J. Eichhorn, *Soft Matter*, 2011, **7**, 303.

76 Y. Habibi, L. A. Lucia and O. J. Rojas, *Chem. Rev.*, 2010, **110**, 3479–3500.

77 M. Hasani, E. D. Cranston, G. Westman and D. G. Gray, *Soft Matter*, 2008, **4**, 2238–2244.

78 Z. Dogic, K. R. Purdy, E. Grelet, M. Adams and S. Fraden, *Phys. Rev. E: Stat., Nonlinear, Soft Matter Phys.*, 2004, **69**, 051702.

79 E. Grelet and S. Fraden, *Phys. Rev. Lett.*, 2003, **90**, 198302.

80 P. Holmqvist, M. Ratajczyk, G. Meier, H. Wensink and M. Lettinga, *Phys. Rev. E: Stat., Nonlinear, Soft Matter Phys.*, 2009, **80**, 031402.

81 N. Krishna Reddy, Z. Zhang, M. Paul Lettinga, J. K. G. Dhont and J. Vermant, *J. Rheol.*, 2012, **56**, 1153.

82 Z. K. Zhang, N. Krishna, M. P. Lettinga, J. Vermant and E. Grelet, *Langmuir*, 2009, **25**, 2437–2442.

83 M. Ripoll, P. Holmqvist, R. Winkler, G. Gompper, J. Dhont and M. Lettinga, *Phys. Rev. Lett.*, 2008, **101**, 168302.

84 P. G. Bolhuis, A. Stroobants, D. Frenkel and H. N. W. Lekkerkerker, *J. Chem. Phys.*, 1997, **107**, 1551.

85 P. Bolhuis and D. Frenkel, *J. Chem. Phys.*, 1997, **106**, 666–687.

86 M. Das, F. C. MacKintosh and A. J. Levine, *Phys. Rev. Lett.*, 2007, **99**, 38101.

87 T. Zhang, J. M. Schwarz and M. Das, *Phys. Rev. E: Stat., Nonlinear, Soft Matter Phys.*, 2014, **90**, 062139.

88 J. R. Rothenbuhler, J.-R. Huang, B. A. DiDonna, A. J. Levine and T. G. Mason, *Soft Matter*, 2009, **5**, 3639–3645.

89 P. G. Bolhuis, A. Stroobants, D. Frenkel and H. N. W. Lekkerkerker, *J. Chem. Phys.*, 1997, **107**, 1551.

90 S. Plimpton, *J. Comput. Phys.*, 1995, **117**, 1–19.

91 M. P. Allen and D. J. Tildesley, *Computer Simulation of Liquids*, Clarendon Press, New York, NY, USA, 1989.

92 A. P. Philipse and A. M. Wierenga, *Langmuir*, 1998, **14**, 49–54.

93 M. J. Solomon and P. T. Spicer, *Soft Matter*, 2010, **6**, 1391.

94 T. Chatterjee and R. Krishnamoorti, *Soft Matter*, 2013, **9**, 9515–9529.

95 J. B. Knight, C. G. Fandrich, C. N. Lau, H. M. Jaeger and S. R. Nagel, *Phys. Rev. E: Stat. Phys., Plasmas, Fluids, Relat. Interdisc. Top.*, 1995, **51**, 3957–3963.

96 E. R. Nowak, J. B. Knight, M. L. Povinelli, H. M. Jaeger and S. R. Nagel, *Powder Technol.*, 1997, **94**, 79–83.

97 C. E. Maloney and A. Lemaître, *Phys. Rev. E: Stat., Non-linear, Soft Matter Phys.*, 2006, **74**, 016118.

98 M. Wyart, H. Liang, A. Kabla and L. Mahadevan, *Phys. Rev. Lett.*, 2008, **101**, 215501.

99 M. J. Solomon and P. T. Spicer, *Soft Matter*, 2010, **6**, 1391.

100 K. H. Kim, M. Vural and M. F. Islam, *Adv. Mater.*, 2011, **23**, 2865–2869.

101 M. K. Shin, J. Oh, M. Lima, M. E. Kozlov, S. J. Kim and R. H. Baughman, *Adv. Mater.*, 2010, **22**, 2663–2667.